Engineering Conferences International
ECI Digital Archives

5th International Conference on Porous Media and Their Applications in Science, Engineering and Industry

Refereed Proceedings

Summer 6-24-2014

HYDRA: Macroscopic modeling of hybrid ablative thermal protection system

G. Pinaud
Airbus Defense and Space

J.M. Bouilly
Airbus Defense and Space

J. Barcena
Tecnalia Research & Innovation

S. Florez
Tecnalia Research & Innovation

B. Perez
Tecnalia Research & Innovation

See next page for additional authors

Authors
G. Pinaud, J.M. Bouilly, J. Barcena, S. Florez, B. Perez, W. Fisher, V. Leroy, D. Bernard, T. Massuti, G. Herdrich, C. Zuber, and W. Rotaermel

Proceedings of the 5th International Conference on Porous Media and its Applications in Science and Engineering ICPM5
June 22-27, 2014, Kona, Hawaii

HYDRA: Macroscopic modelling of Hybrid Ablative Thermal Protection System

Pinaud G. and Bouilly JM.
Airbus Defense and Space, F-33185 Saint Médard en Jalles, France
Barcena J., Florez S. and Perez B.
Tecnalia Research & Innovation, Mikeletegi Pasealekua, 2, Donostia-San Sebastian, Spain
Fisher W.
Airbus Defense and Space, D-28199 Bremen, Germany
Leroy V. and Bernard D.
ICMCB-CNRS Centre National de la Reserche Scienfitique, F-33608 Pessac, France
Massuti T. and Herdrich G.
Institute of Space Systems (IRS), D-70569 Stuttgart, Germany
Zuber C. and Rotaermel W.
Deutsches Zentrum fuer Luft- und Raumfahrt, D- 70569 Stuttgart, Germany

ABSTRACT

In the framework of HYDRA, an European funded program, technological solutions of hybrid Thermal Protection System (TPS) are developed. This advanced shielding relies on the hybridization of upper lightweight porous ablative material and inner Ceramic Matrix Composite (CMC) bonded together with a novel high temperature adhesive. The aerial mass optimization of the full TPS requires a controlled reduction in the ablative material thickness to reach high operating temperature configuration of the CMC. Therefore, radiative heat transfer takes place in a thin layer of ablator and becomes a major contributor to the elevation of the interface temperature. In this paper we develop an high fidelity radiative transfer in porous carbon fibers charring and ablative material. Specific elementary characterization, plasma test campaign and numerical simulation are scheduled to feed this radiative heat transfer model.

INTRODUCTION

The FP7 Space Project HYDRA is an European funded program that aims at developing novel solution in term of advanced TPS associated to a demonstration of Technology Readiness Level (TRL) 4. This advanced hybrid heat-shield design and development is being carried out through ten mix organizations (small and medium, large enterprise), public entities-universities and research centers (Tecnalia, Airbus Defence and Space, HPK, HPS, DLR, IRS, ICMCB, INCAS, Democritos) spread over six European countries. Most of the actual commercial reentry or space exploration missions rely on state of the art pure ablative material such as PICA (Phenolic Impregnated Carbon Ablator). In order to withstand more and more severe oxidative and high temperature environment due to changing strategy and under increasingly demanding economical constraints, it worth to consider innovative solutions of TPS. The hybrid concept consists in the design and the integration of a dual TPS resulting on the overlapping of an external ablative layer with a CMC thermo-structural core. System analysis [1], demonstrated a potential 43 % of aerial mass saving. This gain could be reached by minimizing the ablator thickness, qualifying high temperature adhesive and by using appropriate Internal Flexible Insulator (IFI). For thin porous ablative material layer, conduction-radiation coupling becomes an important heat transport mechanism at high temperature such as met during an high speed return from LEO or LLO orbit trajectory on Apollo like vehicle Fig. 1. Heat transfer by thermal conduction and radiation is therefore investigated through numerical experiments and by comparison with the plasma measurements in the ablative material. After describing the theoretical thermo-chemical model for heat conduction in a porous material undergoing surface oxidation, recession and thermal decomposition of the organic matrix, the conduction-radiation coupling macroscopic model is developed.

NOMENCLATURE

c	Specific heat capacity, [kJ/kg/K]
Δ	Incident/ scattered ray beam, [-]

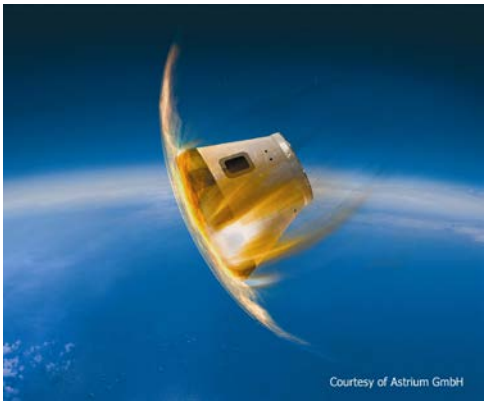

Figure 1. The CTV/ARV vehicle

Φ	Scattering phase function, [-]
H_p	Heat of pyrolysis, [kJ/kg]
h_g	Pyrolysis gas enthalpy, [kJ/kg]
I_ν	Spectral radiative intensity, [W/m^2/micron/sr]
$I_{0,\nu}$	Black Body intensity, [W/m^2/micron/sr]
k	Thermal conductivity, [kW/m/K]
κ_ν	Spectral absorption coefficient,[m^{-1}]
$\dot{m}_g$	Pyrolysis mass mass flow rate, [kg/m^2/s]
Ω	Solid angle, [sr]
ρ_v	Virgin density, [kg/m^3]
ρ_c	Charred density, [kg/m^3]
σ_ν	Spectral scattering coefficient,[m^{-1}]
T	Temperature, [K]
q_r	Radiative heat flux, [kW/m^2]
CMC	Ceramic Matrix Composite
LEO	Low Earth Orbit
LLO	Low Lunar Orbit
TPS	Thermal Protection System
TRL	Technology Readiness Level

I. Equilibrium equations for a porous charring ablative material

The Asterm™ material (manufactured by Airbus Defense and Space) has been selected as the most promising porous charring ablator to fulfil the hybrid TPS mission requirements. When associated with Sicarbon™ as a high TRL Ceramic Composite Ceramic this two material will constitute the hybrid TPS. Asterm™ is a very lightweight ablative material based on a carbon fiber rigid preform, impregnated with phenolic resin. The micro-structure before and after impregnation with the organic matrix appears to be very porous (see Fig. 2) .

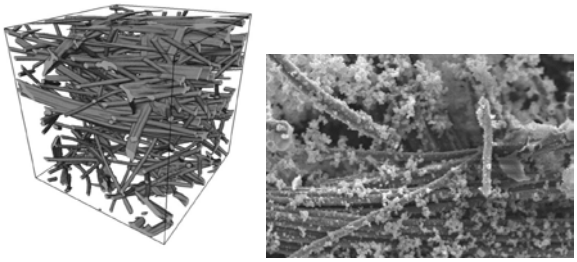

a) Rigid carbon fiber preform before impregnation **b) Rigid carbon fiber preform after impregnation**

Figure 2. Asterm porous microstructure

A. Pyrolysis

When submitted to high heat load and temperature the organic matrix (phenol formaldehyde synthetic polymer (Fig. 3)) starts to decompose in a complex chemistry gas and a solid phase carbonaceous residue. The apparent bulk density of this more porous medium is decreasing. Although much higher fidelity pyrolysis model exist [2], a simple en-

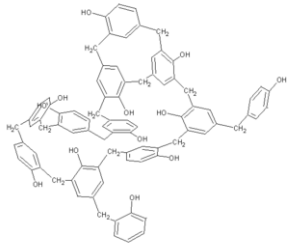

Figure 3. Chemical structure of the phenolic resin

gineering macroscopic approach accounting for mass loss, internal gas flow is used as a baseline and is described hereunder. The internal chemistry and structural transformation kinetics can be modelled by a multi-species Arrhenius law (Eq. 2) with α being the generalized density:

$$\alpha = \frac{\rho - \rho_v}{\rho_v - \rho_c} \tag{1}$$

$$\frac{\partial \alpha_i}{\partial t} = A_i \rho_v^{1-N_i} (\rho_v - \rho_c)^{N_i - 1} (1 - \alpha_i)^{N_i} e^{-\frac{E_i}{RT}} \tag{2}$$

The terms A_i, N_i, E_i respectively pre-exponential factor, reaction order and activation energy can be experimentally identified by thermogravimetry analysis. From the individual species degradation, the expression of the total density variation can be defined:

$$\rho = \rho_v - \sum_i \Delta\rho_i \alpha_i \tag{3}$$

During the thermochemical degradation and following the density change inside the material, the pyrolysis gas products can percolate through the pore. If we assume that the change in gas mass rate is smaller than the bulk density change, the steady state assumptions hold, and the mass conservation can be written as in Eq. 4:

$$\nabla . \dot{\bar{m}}^g + \dot{\rho} = 0 \tag{4}$$

In this equation $\bar{m}^g$ is the gas mass flow rate, which is a vector quantity. As a first approximation the pyrolysis gas are supposed to obey the perfect gas law. The Darcy's equation for the gas momentum conservation can be applied to relate the gas pressure P and the gas mass flow rate, via the expression Eq. 5:

$$\dot{\bar{m}}^g = -K_p \nabla P \tag{5}$$

The parameter K_p is the pressure conductivity which can be defined as a function of the temperature and the pressure (Eq. 6).

$$K_p = \frac{M^g \beta P}{\mu^g R T} \tag{6}$$

The molecular mass M^g, the dynamic viscosity μ^g and the perfect gas constant R (=8.31447) are constant, while the permeability β varies with the porosity of the material. The pyrolysis gas composition and therefore its transports properties are the results of an equilibrium chemical computation based on the atomistic composition of the material in the virgin and charred state. During pyrolysis, not only the density of the material changes, but also the other material properties. These material properties are obtained by interpolation. The interpolation takes place between a so called virgin state and a charred state. The interpolation parameter is the generalized density α. For example, the thermal conductivity tensor k can be expressed either linearly dependant on a or in a more general form (Eq. 7) as combination of the virgin and the charred state.

$$k = f_v(a,T) k_v + f_c(a,T) k_c \tag{7}$$

Together with the density of the virgin material ρ_v and the actual density during the analysis, the porosity Ω can be calculated, using Eq. 8. It can be measured experimentally with mercury intrusion porosimetry techniques.

$$\Omega = \Omega_v + (1 - \Omega_v) \frac{\rho_v - \rho}{\rho_v} \tag{8}$$

The permeability of the material also evolves as the density is decreasing or more exactly as a linear function of the porosity (Eq. 9):

$$\beta = \beta_v \frac{\Omega}{\Omega_v} \tag{9}$$

Measured by Differential Scanning Calorimetry (DSC) or Hot Disk techniques the thermal capacity of the material undergoing pyrolysis is assumed varying linearly with the density (or similarly with a as expressed in Eq. 10:

$$\rho c = \rho_v c_v - \alpha(\rho_v c_v - \rho_c c_c) \tag{10}$$

Pyrolysis phenomena in organic phenolic based material is generally an endothermic process. This heat of pyrolysis shall not be included in the measured capacity which must be the true reversible heat capacity. The heat of pyrolysis $\bar{H}_p$ can be either directly measured with Modulated Differential Scanning Calorimetry or expressed as an energy conservation equation between the solid virgin, charred phase and the pyrolysis gas phase. Then, the expression of the heat of pyrolysis H_p is:

$$\bar{H}_p = h_g - \frac{\rho_v h_v - \rho_c h_c}{\rho_v - \rho_c} \tag{11}$$

In Eq. 11, the specific enthalpy of the pyrolysis gas h_g is computed under chemistry equilibrium assumption.
To finalize the themo-chemical decomposition and phenomenological description of an elementary volume of porous material undergoing pyrolysis, gas diffusion and percolation inside the open pore, it is necessary to solve the energy balance equation (Eq. 12).

$$\rho c \frac{\partial T}{\partial t} - \bar{H}_p \frac{\partial \rho}{\partial t} = \nabla . (k \nabla T) - \dot{m}_g \nabla h_g - \nabla q_r \tag{12}$$

The right hand-side term ∇q_r represent the source term due to the radiative heat transfer. This term will be developed in the section II. The time variation of the temperature is link to the pyrolysis either endo or exothermic reaction ($\bar{H}_p \frac{\partial \rho}{\partial t}$), the phonic conduction through the Fourier law ($\nabla . (k \nabla T)$), and the convected energy carried by the pyrolysis gas percolation ($\dot{m}_g \nabla h_g$). Assuming the pyrolysis gas are in thermal equilibrium with the solid phase there is no need to define any convective pore scale heat transfer between the different phase.

B. Boundary conditions

During an hypersonic atmospheric re-entry, the outer surface of the thermal protection system is exposed to extreme environment (high temperature, chemically reactive dissociated air plasma, and mechanical aerodynamic stress). Inside the boundary layer, several phenomena take place such as thermal and mass diffusion, but also convective transfer due to the wall recession. Indeed, the gas-solid interface is recessing because of heterogeneous oxidative reactions, sublimation reactions, melting and mechanical removal like spallation. The pyrolysis gas percolating through the porous material are also interacting with the boundary layer once they reach this interface. This interaction, known as the blowing effect can significantly reduce the convective heat transfer by modifying the incoming flow composition and by thickening the boundary layer. All this phenomena are summarize in Fig. 4 .

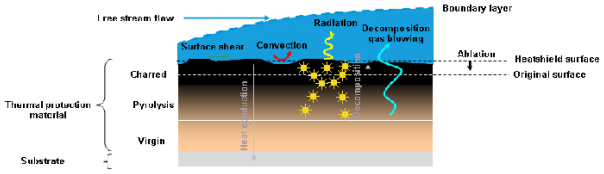

Figure 4. Gas surface interaction for porous charring ablative material

The simplest way to model this gas surface interaction is to express the applied heat flux q in an enthalpy form (Eq. 13) where H_a designates the recovery flow enthalpy, H_w represents the enthalpy of the mixture at the wall pressure and temperature (P_w, T_w) and C_h stands for the convective heat transfer coefficient.

$$q_1 = C_h(H_a - H_w) \tag{13}$$

$$q_2 = -\rho_c \dot{S}_c H_c \tag{14}$$

$$q_3 = C_h B\,(H_c - H_w) + B\,(h_g - H_w \tag{15}$$

$$q_{applied} = q_1 + q_2 + q_3 + q_r \tag{16}$$

The Eq. 14 represents the amount of energy removed due to the recessing surface. The terms B_c, B_g in Eq. 15 are the dimensionless mass rate flow respectively of ablation products and pyrolysis gas products. The coefficient B_c is actually a precomputed table based on thermochemical equilibrium between solid carbon and a gas mixing incoming air from the boundary layer with the pyrolysis gas products. Because the system is assumed to be at thermochemical equilibrium, the reaction are limited by the diffusion process in the boundary layer. The mass diffusion coefficient is implicitly taken equal to the heat transfer coefficient, by imposing a Lewis number equal to 1. The surface recession rate is a 3 dimensional look up table as presented in Eq. 17. An example of simplified table is given in Fig. 5 where only 2 pressures values are selected to make the figure more readable. At relatively low temperature, the oxidation plateau is in a diffusion limited regime. At higher temperature, the sublimation regime is activated and equilibrium pressure composition is therefore dependant on the pressure.

$$B_c = B_c\,T, P, log(P/P_{ref} \tag{17}$$

The blowing effect of the pyrolysis gas on the convective heat transfer is modelled through the λ parameter depending in first approximation, on the boundary layer regime (laminar or turbulent) (Eq. 18).

$$\frac{C_h}{C_{h0}} = \frac{2\lambda B_0}{e^{2\lambda B_0} - 1} \tag{18}$$

In Eq. 18 the term B_0 represents the dimensionless total unblocked mass rate injected in the boundary layer due to ablation and pyrolysis gas.

Finally, the total applied heat flux at the interface between the porous material and the boundary layer is the sum over the convective, diffusive, chemical and radiative contributions. This latest radiative contribution will be detailed in II since some particular attention must be paid when defining boundary radiative conditions on semi-transparent participating media.

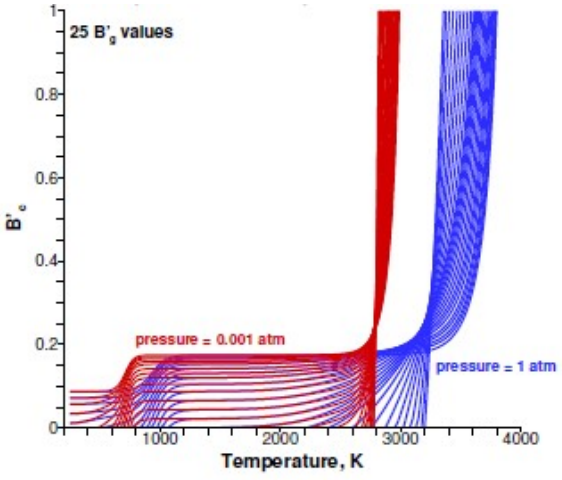

Figure 5. Dimensionless mass flow rate (B_c) for pure carbon in air

II. Radiative heat transfer model

In this section, radiative heat transfer model for semi-transparent, participating, charring and ablative porous material are described. The conduction and radiation coupling mechanism is normally taken into account by a temperature dependent effective conductivity, by making the optically thick material approximation. The effective thermal conductivity (apparent conductivity combining conduction, radiation, internal porous convection) is measured by standard experimental methods (guarded hot plate, laser flash analysis). The conduction only contribution is isolated neglecting convective transfer mode and using the approximate solution for the radiation mode. A low fidelity equivalent diffusion model (Rosseland diffusion equation) is implemented based on the measurement on PICA material (comparable to Asterm™). This approximation is valid in case of an optically thick material such like in [3] . The Rosseland radiative diffusion equivalent conductivity is presented in Eq. 19:

$$k_R = \frac{16\sigma T^3}{3\beta_r} \tag{19}$$

In the Rosseland radiative conductivity equation (Eq. 19) the parameter β_R is the apparent extinction coefficient which can defined as the sum of the absorption and scattering coefficient. For PICA material, the solar furnace test campaign analyse concludes that the apparent extinction coefficient was approximatively $7.7m^{-1}$. The Rosseland radiative conductivity (Fig. 6) is therefore computed with this value both for the virgin and charred material.

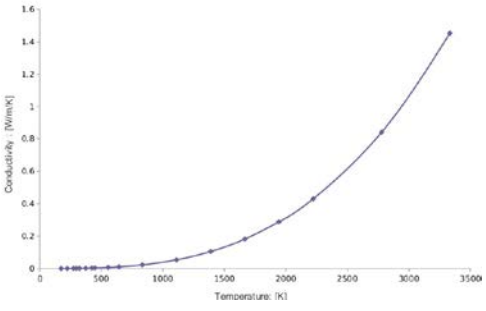

Figure 6. Rosseland radiative conductivity

A. Applied Mie theory for porous fibers media

In order to improve the predictability capability of the engineering model, a radiation balance for a generic absorbing/emitting/scattering porous medium [4] is implemented. A realistic wave-length dependent thermo-optical properties are calculated.The spectral absorption

and scattering are based on the radiation properties of a carbon fiber, obtained by Mie theory for an infinite pure carbon cylinder and homogenized for the whole material [5]. The homogenization procedure considered a fully isotropic, randomly non intersecting fibers aggregate with similar apparent bulk density than a raw carbon felt. The theoretical homogenized properties of the synthetic material is then scaled by the measured extinction coefficient realised on real material. The spectral radiation coefficient present a smooth and nearly monotonous variation on a the IR spectral band (Fig. 7). Because of the material micro-structure is evolving as the pyrolysis front is going deeper in the shield, it would have been more realistic to consider two sets of radiative coefficient, one for each material state. However, the elementary characterization at low temperature of the virgin extinction coefficient seems unachievable. Moreover, the radiative heat transfer is only efficient at high temperature where the fully virgin material is only a theoretical view. The impact of the spectral radiation coefficients and

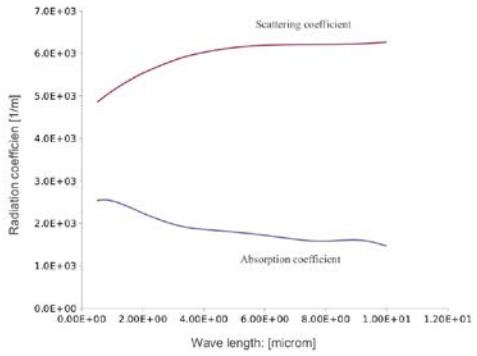

Figure 7. Scaled absorption and scattering radiative coefficient

phase function is also investigated. The scattering phase function will be simplified so that it is a function of the scalar product of the incoming and outgoing direction. Thus, the phase function can be described as a function of the angle between these two directions. In a similar way than for the radiative absorption and scattering coefficient the scattering phase function is not dependant on the decomposition state. Three scattering phase functions are implemented: an isotropic, a linear backward and forward anisotropic phase function (Fig. 8). The predicted thermal response are compared against the temperature measurements obtained during the high enthalpy plasma test campaign.

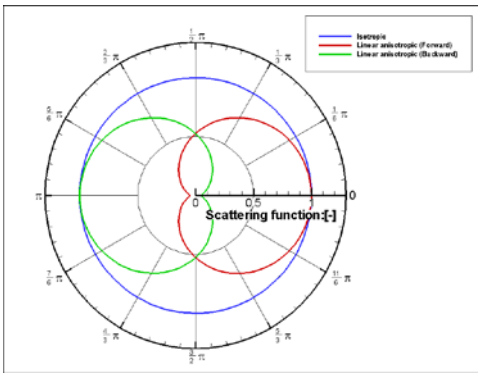

Figure 8. Isotropic and linear anisotropic scattering phase function

B. Radiative energy balance equation

The radiation transport equation (Eq.20) is simultaneously solved with the standard energy balance equation (Eq.12) in order to tackle the fully coupled radiation-conduction problem.

$$\frac{\partial I_\nu}{\partial t} = -(\kappa_\nu + \sigma_\nu) I_\nu + \kappa_\nu I_{0,\nu} + \frac{\sigma_\nu}{4\pi} \int_{\Omega=4\pi} I_\nu \Phi(\Delta_i \rightarrow \Delta) d\Omega \qquad (20)$$

And,

$$q_r = \int_\nu \int_\Omega I_\nu d\Omega d\nu \qquad (21)$$

The source term, linked to the internal volumetric radiative heat transfer q_r, is then added to the standard energy balance equation. The simulations are performed with the Samcef Amaryllis module. The code uses a 3D spectral ray-tracer to solve the coupled conduction-radiation balance in charring ablative materials. The radiative conductive equations are solved after an homogenisation step in temperature and density for the participating element. Thus reducing the finite element to an equivalent finite volume element. The rays are launched from every element and every external face, and they are traced through the structure until they are absorbed or leave the medium. The ray-tracing method will loop over all the active external faces and all the volume elements. On every face/volume a random number generator will be used to determine:

- The point of origin,
- The wave-length of the emitted ray,
- The direction of emission,
- The direction of emission.

When a ray is either absorbed or has left the volume the next ray will be launched, until all volumes/faces have launched all their rays. All the external faces of the finite element mesh will participate in the ray-tracing algorithm. If the faces are not explicitly defined as the main gas-solid interface of the domain, they act as a pure specular reflectors. In our specific case (for a very low density carbon fibers based material) we assume that the refraction index of 1 inside the solid phase. At the interface between the gas and porous media, we also assume that the assumptions of Fresnel boundary conditions for a dielectric can hold. When a ray impacts the interface between two materials (Fig. 9), with two different refraction indices n, it is either reflected or transmitted. If the ray is transmitted the incident angle will not be the same as the angle of transmission. The relation between the two angles is given in Eq. 22:

$$n_1 sin(\theta_1) = n_2 sin(\theta_2) \qquad (22)$$

The refraction index being equal to 1, the spectral reflectivity of the

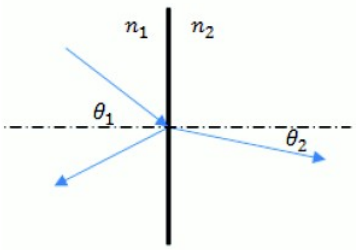

Figure 9. Isotropic and linear anisotropic scattering phase function

interface is equal to 0.

III. Plasma test campaign simulation

Once the mission of interest for this hybrid TPS have been selected (re-entry trajectory from LEO or LLO), a preliminary characterization of the flow environment is simulated, defining a corridor of potential stagnation total heat flux and pressure (see Fig. 10). The flight conditions are then compared to the plasma environment (Fig. 10) that can be simulated in the IRS Magnetic Plasma Generator (MPG) (Fig. 11). Even if the attainable heat flux and pressure on ground are lower than the flight predictions, the plasma enthalpy is large enough to recreate representative chemical environment (oxidation and sublimation). A 2D axi-symmetric thermal Finite Element model of the test article is built within Samcef Amaryllis to simulate the behaviour of the stack of material under the plume plasma jet (Fig. 12). Numerical thermocouples located at the same locations than real ones can therefore be

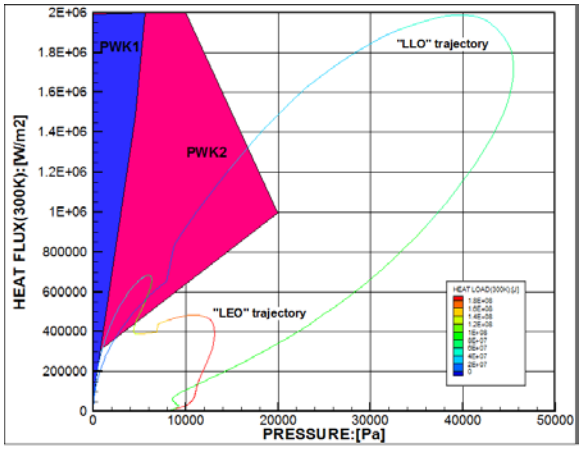

Figure 10. Aerothermodynamic environment on two referenced missions

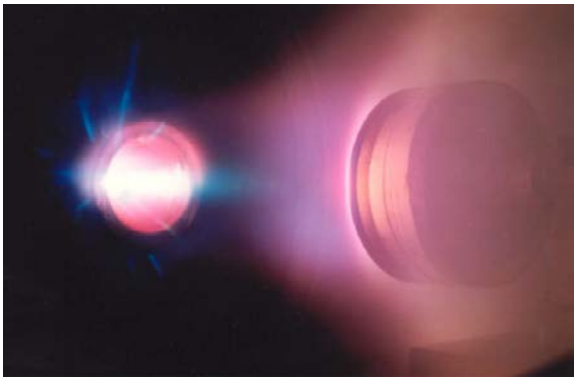

Figure 11. Hybrid article under MPG plasma facility at IRS

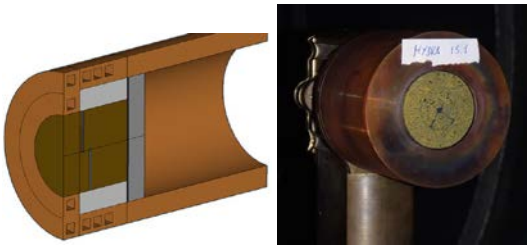

Figure 12. FE model and test article configuration

compared with the measurements. The location of real thermocouples are inspected through computer tomography (Fig. 13). Both simulated temperature and dimensionless density time history at 10 fix locations in depth (including the position of the thermocouples) for the baseline (simple Rosseland radiative diffusive model) are presented on FIg. 14. The theoretical thermocouples are automatically set to zero when the wall is reaching the pseudo-thermocouples location. Removing the Rosseland diffusive term from the apparent conductivity, and applying the high fidelity radiative model (with iso, backward and forward linear anisotropic scattering, Fig. 15) changes drastically the temperature at the outer wall and the few first outer millimetres of the temperature in-depth distribution. Indeed, with the high fidelity radiative model, the wall temperature is shift by more than 400 C. This strong effect indicates the importance of the extinction coefficient value which might be larger than the one measured in [3]. Usually the wall temperature is measured by a bi-chromatic pyrometer and considering the large thermal gradient near the surface, the accuracy of this measurements on very porous material could be questionable. The temperature distri-

Figure 13. Thermocouple localization through X-Ray Computer tomography

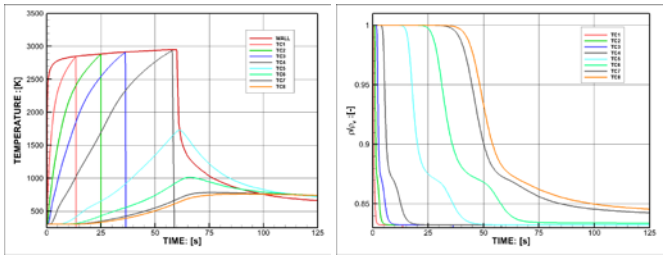

Figure 14. Temperature and dimensionless density time history for the reference model (Rosseland approximation)

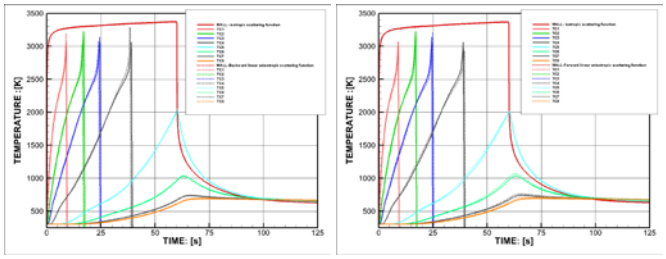

Figure 15. Temperature time history for iso,backward (left) and forward scattering (right) radiative model

bution for linear backward and forward anisotropic scattering is very close to the isotropic configuration (Fig. 15). Even the thermal response seems not sensitive to the scattering phase function, a charred state dependency could be implemented to take into account the microstructural and morphological change that occur at fibers scale during the pyrolysis. Since the density is affected by the temperature and the heating rate, the radiative heat transfer model also entails some modifi-

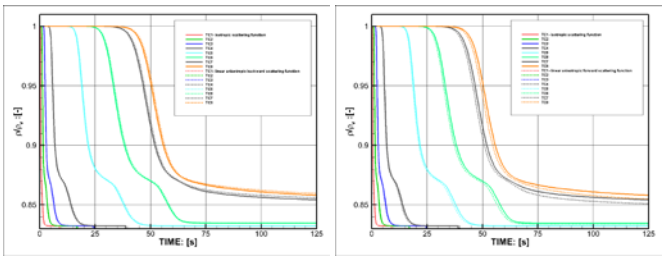

Figure 16. Dimensionless density time history for iso,backward (left) and forward scattering (right) radiative model

cation into the density profile (Fig. 16). The large increase temperature at the wall, driven by the absorption and scattering properties of the fibers is shifting the ablation regime from a limited diffusion to the sublimation. Under chemical equilibrium this has tremendous consequences on the recession (Fig. 17). However, this predicted recession (with high fidelity radiative model) is not consistent with the experimental observations. The recession measurement do not question the validity of the model itself but more the thermo-optical properties that has been estimated from literature for this material. A sensitivity analysis on the radiative extinction coefficient spectral distribution is currently being carried out in order to retrieve properties that could match with the plasma test thermochemical characterization.

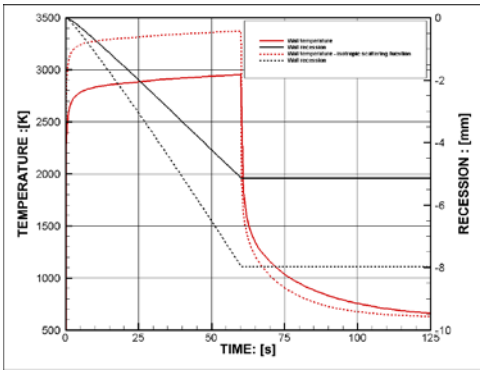

Figure 17. Ablation rate for Rosseland radiative diffusion approximation and for high fidelity radiative model (isotropic scattering)

Conclusions

The FP7 project HYDRA aims at identifying a new TPS concept that combines a low density ablator and an underneath hot substructure. Main anticipated advantages are focused on mass reduction as compared with a solution based on a single ablator solution, while increasing the temperature limits as compared with a re-usable system. The mission and flight envelop are selected and requirements defined. Future effort will focus on the completion of the verification plan including further characterization in Plasma Wind Tunnel. System analysis carried-out with regards to the mass saving compared with a full ablative concept attests achievable benefit. Optimized design of hybrid TPS lead to thin layer or ablative material, where radiative heat transfer play a greater role compared to stand-alone ablator. Therefore, a special effort have been done during the Hydra project to implement such high fidelity radiative model with the aim to predict with more confidence the bond-line and adhesive temperature. Indeed, highly reliable prediction of this temperature is needed in order to insure that the high temperature adhesive integrity criteria is never reach. A standard thermochemical model of porous charring fibrous media model provides a solid framework for further sensitivity analysis of the newly developed high fidelity radiative model. This model, base on Mie theory is currently limited by the lack of thermo-optical properties of such porous fibrous ablator. A specific effort has to be done on thermo-optical characterization of Asterm™. This problematic is currently addressed experimentally at INRIA. Ways how to improve this properties prediction are identified and shall also include the combination of fibers and matrix morphology. Furthermore, theoretical activities are conducted by the ICMCB research center to demonstrate the validity of a downscaling procedure [6] that aim to capture micro-scale effect of pyrolysis phenomena. Morphological simulation of the material will be performed at micro-scale level so that important information could serve to improve the engineering model.

Acknowledgements

The research leading to these results has received funding from the European Union Seventh Framework Programme (FP7/2007-2013) under grant agreement n 283797.

References

[1] Barcena, J., "Novel Hybrid Ablative-Ceramic Heatshield for Earth Atmospheric Re-Entry," *European Conference on Spacecraft Structures, Materials and Environmental Testing*, April 2014.

[2] Weng, H., "Multi-dimensional modeling of charring ablators," *44th AIAA Thermophysics Conference*, June 2013, AIAA 2013-2635.

[3] White, S., "Radiation Testing of PICA at the Solat Power Tower," *10th AIAA/ASME Joint Thermophysics and Heat Transfer Conference*, 28 June-1 July 2010, AIAA 2010-4665.

[4] Siegel, R. and Howell, J. R., *Thermal Radiation Heat Transfer*, Vol. 3, 1971, pp. 277–349.

[5] Hulst, Hendrick, C. V. D., *Light Scattering by Small particles*, Dover, New York, 1981.

[6] Leroy, V., "A downscaling procedure for transport in C/R Thermal Protection System," *11th AIAA/ASME Joint Thermophysics and Heat Transfer Conference*, June 2014.